Quasi-stationary waves and their impact on European weather and extreme events

Received: 14 November 2017 | Revised: 05 April 2018 | Accepted: 06 April 2018 | Published on: 21 November 2018

DOI: 10.1002/qj.3310

RESEARCH ARTICLE

Quarterly Journal of the Royal Meteorological Society RMetS

Quasi-stationary waves and their impact on European weather and extreme events

Gabriel Wolf[1,2] | David J. Brayshaw[1,2] | Nicholas P. Klingaman[1,2] | Arnaud Czaja[3]

[1]Meteorology Department, University of Reading, Reading, UK
[2]National Centre for Atmospheric Sciences, University of Reading, Reading, UK
[3]Space and Atmospheric Physics, Imperial College, London, UK

Correspondence
Gabriel Wolf, Department of Meteorology, Earley Gate, University of Reading, P.O. Box 243, Reading, Berkshire RG6 6BB, UK.
Email: g.a.wolf@reading.ac.uk

Funding information
NERC ODYSEA project (grant number: NE/M006085/1) and a NERC Independent Research Fellowship (NE/L010976/1),

Large-scale, quasi-stationary atmospheric waves (QSWs) have long been known to be associated with weather extremes such as the European heatwave in 2003. There is much debate in the scientific literature as to whether QSW activity may increase under a changing climate, providing a strong motivation for developing a better understanding of the behaviour and drivers of QSWs. This paper presents the first steps in this regard: the development of a robust objective method for a simple identification and characterization of these waves. A clear connection between QSWs and European weather and extreme events is confirmed for all seasons, indicating that blocking anti-cyclones are often part of a broader-scale wave pattern.

Investigation of the QSW climatology in the Northern Hemisphere reveals that wave activity is typically strongest in midlatitudes, particularly at the exit of the Atlantic and Pacific storm track, with weaker intensities in summer. In general, the structure of individual QSW events tends to follow the climatological pattern, except in winter where the strongest and most persistent QSWs are typically shifted polewards, indicating a distinct evolution of the "strongest" QSW events. Modes of interannual variability are calculated to better understand their importance and connection to European temperatures and to identify relevant QSW patterns. This analysis highlights that European winter temperatures are strongly associated with the meridional location of QSW activity whereas high European summer temperatures are associated with increases in the overall intensity of midlatitude QSW activity.

QSWs are shown to be strongly connected to commonly used indices to describe the large-scale atmospheric circulation (NAO, AO, Niño 3.4, PNA) but offer a more direct link to understanding their impact on regional weather events. It is therefore hoped that objective identification of QSWs will provide a useful new viewpoint for interpreting large-scale weather alongside more traditional measures.

KEYWORDS

climate variability, European temperature, global pattern indices, quasi-stationary wave, weather extremes

1 | INTRODUCTION

Midlatitude weather is typically dominated by quickly moving and evolving synoptic-scale cyclones and anticyclones on sub-weekly time-scales. However, many periods of extreme European weather (e.g. heatwaves) are associated with a relative stalling of these conditions – that is, periods of persistent weather regimes on time-scales of several days to about two weeks (Horel, 1985; Black *et al.*, 2004). These persistent regimes are frequently associated with so-called "blocking

anticyclones", which are known to be relevant at the exit of the North Atlantic storm track (Masato *et al.*, 2014).

However, strong localized blocking anticyclones over Europe are commonly part of a much larger pattern, associated with a slowly evolving, longitudinally extended quasi-stationary wave (QSW; e.g. Nakamura *et al.*, 1997). Similar connection can be shown for blocking highs at the end of the Pacific storm tracks, associated with droughts in California (Teng and Branstator, 2017) or extreme cold events in North America (Carrera *et al.*, 2004; Whan *et al.*, 2016), which also can be associated with a larger-scale wave pattern (Xie *et al.*, 2017). Previous studies have further suggested that periods of increased QSW activity lead to more extreme weather conditions, whereas periods of attenuated QSW activity lead to "near-average" weather (Screen and Simmonds, 2014).

On a more climatological level, very persistent or recurrent QSWs with the same phasing can lead to weather extremes and dominate the flow regime of a complete season (Trenberth and Guillemot, 1996; Pan *et al.*, 1999). In summer, extreme heat waves and droughts can be linked to strong blocking anticyclones that can be part of a wider wave signal (Kornhuber *et al.*, 2017).

Petoukhov *et al.* (2013) introduced the idea of quasi-resonant amplification as a specific class of QSWs, based on the model studies of circumglobal teleconnections of QSWs (Branstator, 2002; Ding and Wang, 2005). Their hypothesis is that a phase-locked quasi-resonant circumglobal wave pattern amplifies strongly, leading to extreme circulation and temperature anomalies. The extent to which this mechanism is relevant for extreme events in general remains unclear.

The low-frequency and large-scale properties of these QSWs makes them relevant for teleconnection patterns. Understanding specific classes of QSW patterns and their drivers can therefore increase prediction skill for weather regimes in regions remote from the wave source. Sato and Takahashi (2006) highlighted the effect of QSWs along the subtropical Asian jet and their relation to midsummer climate over Japan and the downstream evolution in the Pacific. Numerical studies of Enomoto *et al.* (2003) show that the Indian monsoon can excite QSWs. Arctic warming and sea-ice extent may have an important effect on the climatology of near-stationary planetary waves (Porter *et al.*, 2012; Cohen *et al.*, 2014; Tang *et al.*, 2014) but there remain open questions about the connection between QSWs and climate change (Walsh, 2014).

Given the recent increase in the availability of high spatial- and temporal-resolution climate data from GCMs and reanalyses, it is both desirable and timely to study the climatological properties of QSWs in detail. While the temporal evolution of waves can be readily visualized by Hovmöller diagrams (Hovmöller, 1949; Glatt *et al.*, 2011) and while Glatt and Wirth (2014) used such diagrams to objectively identify and investigate Rossby wave behaviour, in using Hovmöller diagrams one loses information about the wave location in the meridional direction. Conversely, representing the wave occurrence of a specific time period by temporally averaging longitude–latitude maps by the use of phase-dependent quantities like the meridional wind can lead to phase cancellation in the case of non-stationary waves and an underestimation of wave amplitude. A way to partly overcome the problem of phase cancellation is to compute composites centred on a fixed phase (ridge or trough) along the direction of the mean flow, similar to themethod used by Catto *et al.* (2010) for a composite of extratropical storms. However, this method is not suitable for calculating a general climatology of waves and even for a composite study (besides losing valuable information about the regional occurrence of the waves) zonally far-elongated waves of different dominant wavenumbers would still be prone to the effect of phase cancellation towards the remote regions from the composite centre. More recently, phase-independent measures like wave activity fluxes (Plumb, 1985; Takaya and Nakamura, 2001) or envelope reconstruction of the meridional wind (Zimin *et al.*, 2003; 2006) have been used. These tools are further developed in this paper to develop an explicit "climatology" of QSWs for the Northern Hemisphere and to explore its climatological properties.

By further exploiting the concept of waveguides, as done in Hoskins and Ambrizzi (1993) or Teng and Branstator (2017), one can identify possible wave paths; this allows a better understanding of teleconnection patterns. However, this paper will focus on the climatology of QSWs and particular interesting QSW patterns. In future work we intend to further explore the connection between specific QSW patterns and the associated waveguides in both reanalysis data and simplified aquaplanet model set-ups.

The remainder of this paper is organized as follows. Section 2 demonstrates the method to calculate QSWs by using a highly amplified extreme wave during the 2003 European heat wave. Section 3 shows the existence of a general connection between QSWs and extreme weather events beyond individual case-studies. This can be used as motivation for a deeper investigation of these QSWs. Therefore the QSW calculation is applied to ERA-Interim in section 4 to get a general climatological understanding of the behaviour of these waves. Section 5 analyses the main modes of variance and covariance between QSW amplitudes and temperature to get a deeper understanding of the differences and impacts of the most relevant QSW patterns. The key conclusions of this paper are summarized in section 6.

2 | DATA AND METHOD

ERA-Interim reanalysis (Dee *et al.*, 2011) is used for all meteorological quanities on a longitude–latitude grid with $0.75° \times 0.75°$ resolution. The data are linearly detrended at each gridpoint over 1979 to 2015.

The upper tropospheric quasi-stationary wave (QSW) is calculated from the anomalous meridional wind v' at 300 hPa. This quantity we seek is a stationary or slowly propagating wave signal and therefore a 15-day lowpass filter is applied to the raw meridional wind, v, to remove the faster-propagating wave signals. The resulting filtered data are subsequently denoted as $\widetilde{v}$. A climatological annual cycle $\overline{\widetilde{v}}$ is then calculated and removed to produce the resulting anomalous meridional wind ($v' = \widetilde{v} - \overline{\widetilde{v}}$) which is then used to calculate the QSW.

The QSW is assumed to consist of the form

$$v'(\lambda) = A(\lambda)\, C(\lambda),$$

where λ is longitude, C is the so-called carrier wave and A is the slowly varying amplitude. The carrier wave is a simple sine function $C = \sin(s\,\lambda)$ with wavenumber s. While C oscillates between positive and negative values, A is non-negative everywhere and varies on a much larger spatial scale than C. In the following, we refer to A as the envelope of the wave. In reality, the wave consists not of a carrier wave with only one specific wavenumber s, but a range of wavenumbers ($s_1 \leqslant s \leqslant s_2$). With $v'(\lambda)$ given and assuming C consists of a specific range of relevant wavenumbers (typically $s_1 \approx 4$ to $s_2 \approx 8$ in midlatitudes), we can calculate the envelope of the wave A.

For this envelope reconstruction, we use the method of Zimin *et al.* (2003), but instead of using a fixed wavenumber range, we choose a latitude-dependent wavenumber range (as in Wolf and Wirth, 2017). The latitude dependence is based on the cosine decay of the main contribution of the power spectra of v'. The power spectra of v' and the consequent choice of the latitude-dependent wavenumber range (and its relation to classic barotropic Rossby wave theory) is discussed in the Appendix.

As an illustration of the method, we show the individual steps of the QSW calculation applied to 9 August 2003 (Figure 1). From the meridional wind (shading in Figure 1a) or geopotential (contour lines), one can by eye easily identify a clear wave pattern in the zonal direction (Figure 1a) which becomes even more clearly visible after applying the 15-day lowpass filter (Figure 1b). The envelope reconstruction captures the region exposed to this wave pattern (Figure 1c). However, the envelope mainly shows high values in the centre of the wave signal and strongly decreasing values towards the meridional edges of the wave. A Hann filter is therefore applied to the adjacent 7.5° latitude (Figure 1d) to slightly increase the meridional dimension of the wave envelope. The envelope for this date represents a very strong wave, which can be seen by the area exceeding the 95th percentile of summer values (thick line in Figure 1d).

The resulting mean climatological pattern of "QSW envelope amplitude" (hereafter "QSW amplitude") in summer and winter is shown in Figure 2 and will be discussed in detail subsequently (section 4).

For the connection beetween QSWs and large-scale weather patterns, we use monthly values of indices for the North Atlantic Oscillation (NAO), the Arctic Oscillation (AO), the Pacific/North America pattern (PNA) and the El Niño Southern Oscillation in the Niño 3.4 region (Niño 3.4), downloaded from http://www.cpc.ncep.noaa.gov/data/ (accessed 13 October 2018). The NAO and PNA indices are calculated based on the Rotated Principal Component Analysis used by Barnston and Livezey (1987), applied to monthly mean standardized 500 hPa height anomalies. The AO index is constructed by a projection of the monthly averaged 1000 hPa height anomalies onto the leading EOF mode, capturing mainly the characteristics of the cold season because of the largest variability.

3 | CONNECTION TO EXTREME EVENTS

In this section, we connect QSWs to extreme weather events. An example of this connection has already been shown for one specific case in Figure 1, which shows the date of peak temperatures during the European heat wave of 2003 (as discussed by e.g. Black *et al.*, 2004). The amplitude of the associated QSW is one of the highest values in summer for the 1979–2015 period in ERA-Interim.

In the following we investigate composites of the 30 warmest and coldest extremes in Europe. Extremes are defined as follows:

(i) We calculate a regionally averaged temperature at 850 hPa for Europe (10°W to 20°E and 40 to 60°N).

(ii) We apply a 7-day running mean to this time series to focus on more persistent extreme events. Tests showed that the results of our analysis were insensitive to the length of this window.

(iii) We then composite the 30 most extreme events of the temperature time series under the condition that the events are separated by at least 10 days. We have done this for all seasons separately (MAM, JJA, SON and DJF). For simplicity, we focus on the summer (JJA) and winter (DJF) seasons, and only briefly discuss the major differences or similarities in the transition seasons.

We then calculate the composite QSW amplitudes for periods where the extreme temperature anomalies occurred (Figure 3). For all seasons, extreme temperature anomalies are connected with extremely strong contemporaneous QSW amplitudes. Further, most of these composites – particularly the extreme warm anomalies in Figure 3b,d – show zonally elongated regions of enhanced QSW amplitudes from the Pacific towards Europe. This indicates that these extreme temperature events are connected not only to a strong local blocking anticyclone, but also to a much more zonally extended and long-lived wave pattern. Furthermore, while extreme cold events in JJA perhaps appear to be more localized phenomena (rather than a zonally extended QSW), it is possible to identify

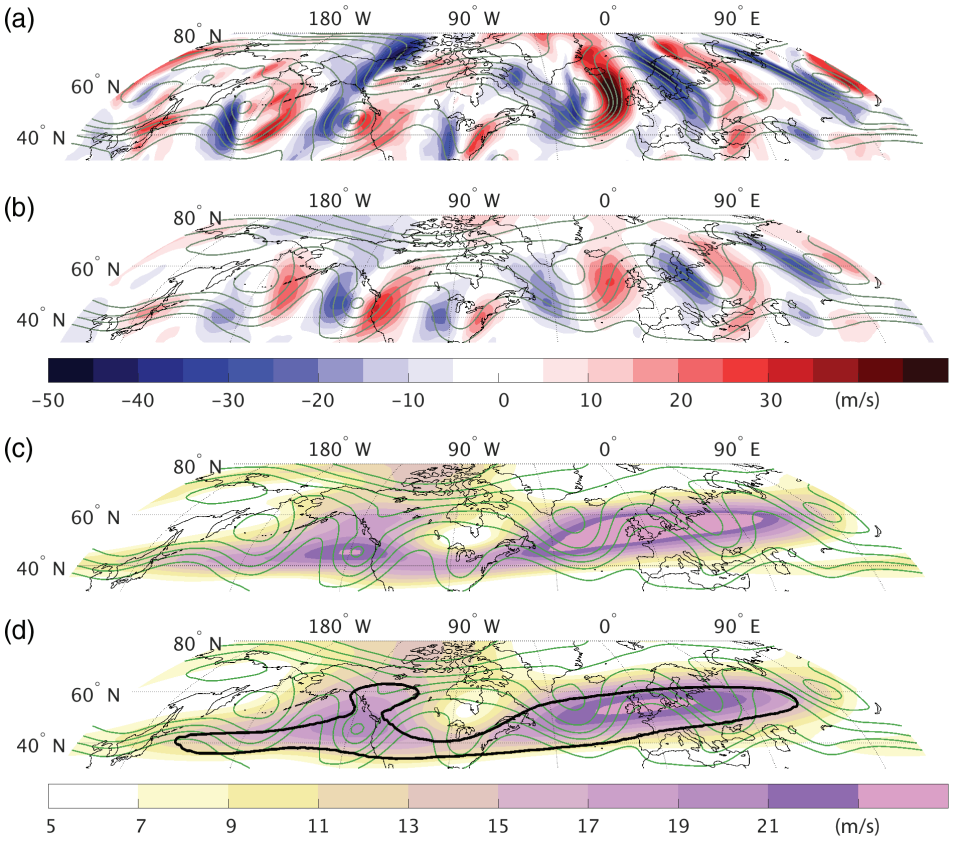

FIGURE 1 Individual steps for the calculation of the quasi-stationary wave at 300 hPa for 0000 UTC on 9 August 2003. (a) meridional wind speed, (b) deviation of the 15-day lowpass filtered meridional wind from the daily climatology, (c) envelope field of the wind field shown in (b), and (d) envelope field after applying a Hann filtering in the meridional direction (all shading, $m\,s^{-1}$). Contour lines show geopotential between 8.8×10^4 and 9.5×10^4 $m^2 s^{-2}$, at intervals 0.1×10^4. The bold line in (d) represents the area exceeding the 95th percentile of envelope values in summer (JJA) [Colour figure can be viewed at wileyonlinelibrary.com]

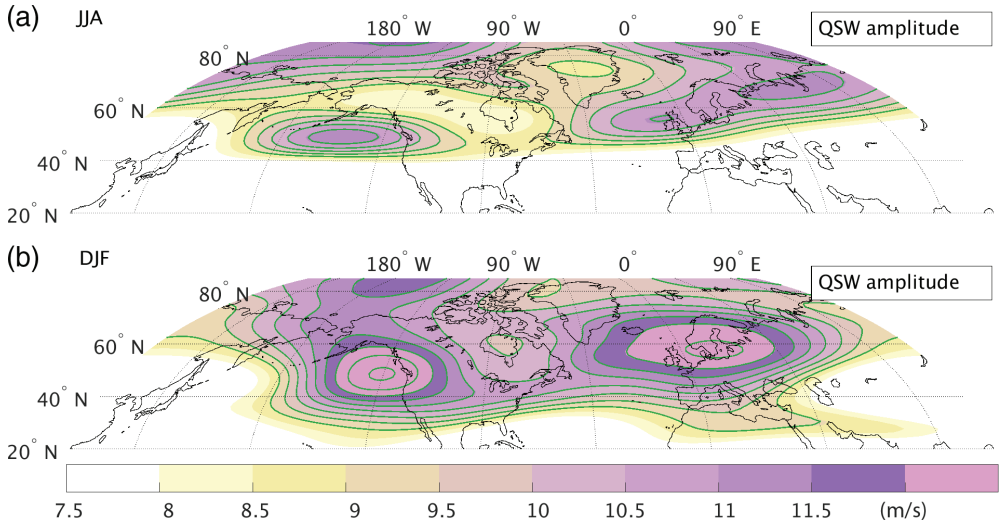

FIGURE 2 Spatial distribution of QSW amplitude during (a) summer (JJA) and (b) winter (DJF). Shaded contours show the QSW envelope amplitude with spacing $0.5\,m\,s^{-1}$, starting at $9\,m\,s^{-1}$ [Colour figure can be viewed at wileyonlinelibrary.com]

a time-delayed signature of zonally elongated QSW amplitudes from the Pacific toward Europe (Figure S1, Supporting information). Therefore, extreme cold events in JJA are also connected with zonally elongated QSWs. We also note that the extreme cold events are associated with QSWs at higher latitudes than the extreme warm events.

An interesting feature of the composites is the almost complete zonal band of anomalously strong QSW amplitudes in JJA for extreme warm events (Figure 3b). This is perhaps consistent with the mechanism of quasi-resonance, suggested by Petoukhov *et al.* (2013). They showed that some extreme events are associated with very strong amplitudes of the

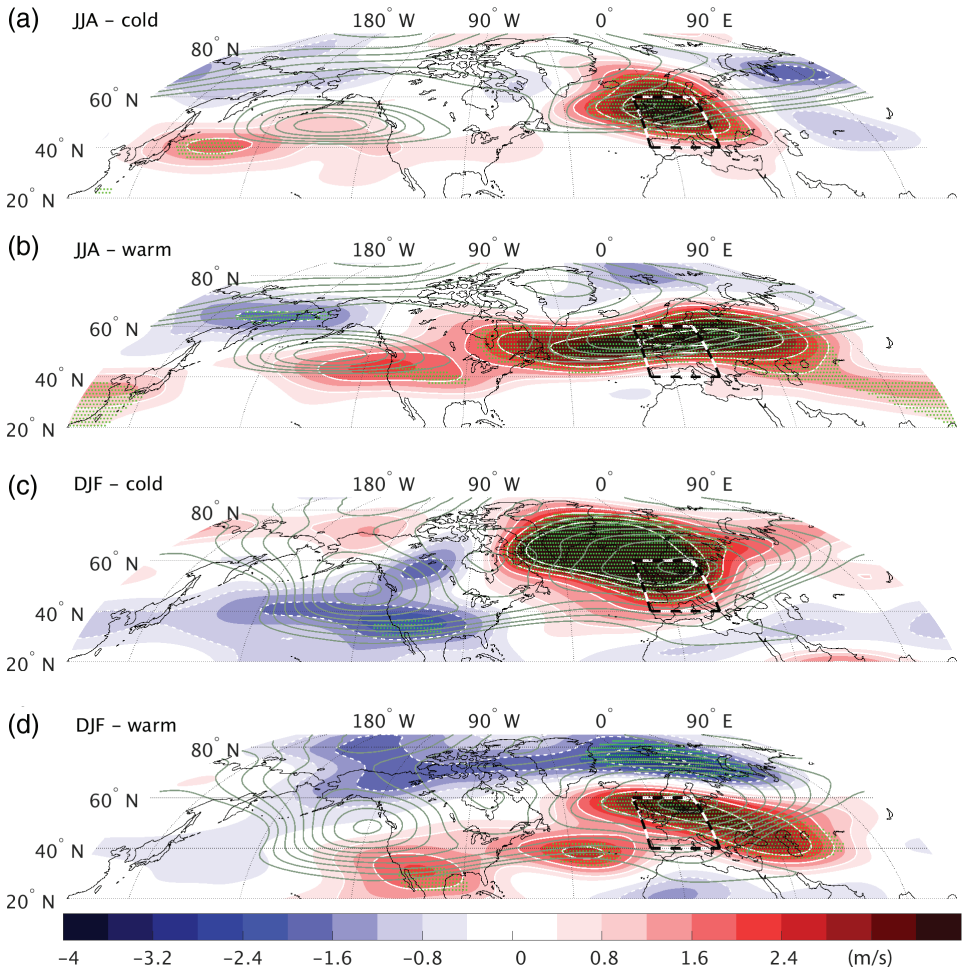

FIGURE 3 Connection between QSWs and extreme temperature anomalies during JJA and DJF. White contours (dotted lines for negative values, solid lines for positive values) and shading shows the anomalous QSW amplitudes (as deviations from daily climatology) associated with: (a) the 30 most extreme cold events during summer (JJA), (b) the 30 most extreme warm events during JJA, (c) the 30 most extreme cold events during winter (DJF) and (d) the 30 most extreme warm events during DJF. Extreme temperature events are defined by a 7-day running mean and a regional average over central Europe (dashed black-white box). Dots show statistical significance, based on the 99th percentile. Contours show the climatological wave amplitude for the associated season, with spacing 0.5 m s^{-1}, starting with 9 m s^{-1} [Colour figure can be viewed at wileyonlinelibrary.com]

meridional wind with specific wavenumbers, derived from a Fourier transform. For most of our extreme composites (i.e. DJF warm, DJF cold, JJA cold in Figure 3) the QSW amplitude anomaly does not complete a full zonal circuit, suggesting a physical interpretation whereby a local amplification of the QSW or downstream development and amplification of the QSW occurs during the extreme temperature events. However, the QSW evolution during some extreme warm anomalies in JJA (14 of the 30 cases in Figure 3b) does suggest a complete zonal band where QSW amplitude exceeds their climatological 95th percentile (and more than 315° of longitude exceeds the climatological 99th percentile).

This is further explored in Figure 4, which shows the temporal evolution of the QSW composite associated with the subsample of 14 from the 30 extreme warm anomalies during JJA. One can see the high values of QSW amplitudes (shading) associated with the warm anomalies over Europe at day 0. Remarkably, these events also show strong temperature anomalies in remote regions, like the US west coast. The strong QSW amplitudes develop at different longitudes simultaneously around 5 days earlier. This simultaneous wave amplification in remote regions appears to further support the quasi-resonance mechanism, although this must be interpreted with some caution due to the temporal filtering of the underlying meridional wind data.

The connection between extreme temperature events and strong QSWs for Central Europe exists not only for the most extreme cases, but also for more moderate temperature variations. In particular, stronger temperature anomalies (both positive and negative) are connected with QSWs whereas days with near-average temperatures are associated with an absence of QSWs (Figure 5). This is also true for the transition seasons, with the spring QSW pattern similar to the winter pattern (Figure 5a) and the autumn QSW pattern similar to the summer pattern (Figure 5b).

Similar results can be derived also for extreme precipitation events, both wet and dry, using the 30 most extreme cases of a 7-day running mean of the total precipitation in the same European region (Figure S2 for JJA and DJF). For all seasons, the dry composites are connected with very strong QSWs,

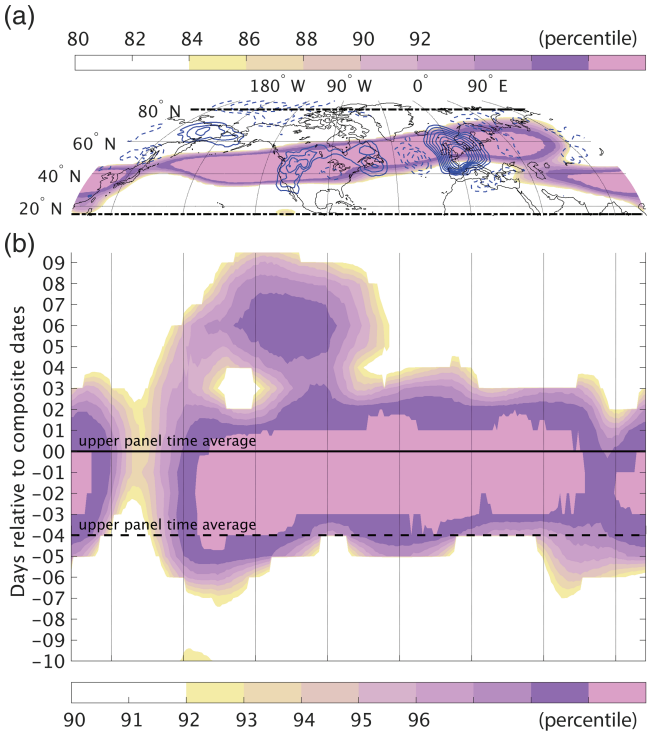

FIGURE 4 Quasi-resonance for the extreme warm anomalies during JJA. Shading shows the the percentile of QSW amplitude, calculated by a Monte Carlo simulation of 5000 composites with 14 events during JJA. (a) shows the time average of the composite dates −4 to 0 (black horizontal lines in (b)). (b) shows the meridional average of the 10 highest percentiles at each longitude for each timelag day. Solid (dash-dotted) contour lines in (a) show positive (negative) averaged temperature anomalies, spaced every 0.5 K, starting with ±1 K [Colour figure can be viewed at wileyonlinelibrary.com]

exceeding the 99th percentile, as are the wet composites, except in winter (DJF). While all other seasons show a highly statistical significant QSW and a large-scale trough over central Europe, the DJF composite shows negative anomalies in the QSW amplitude and zonal flow (not shown).

The preceding analysis demonstrated that extreme European temperature anomalies tend to occur during strong QSWs. However, this does not imply that a strong QSW always leads to a strong temperature anomaly. To explore this, we calculated the temperature anomalies associated with the 30 strongest QSWs in the Atlantic–European region (45°W to 45°E and 40 to 60°N).

Strong QSWs are indeed typically associated with strong European temperature anomalies in JJA and DJF (Figure 6) as well as for the transition seasons (not shown). The connection between QSWs and temperature extremes works in both directions. A gridpoint correlation between the modulus of temperature anomalies and anomalous QSW amplitudes further reveals that this connection extends to large parts of the Northern Hemisphere (not shown) and in particular for Europe during JJA. Similar results can be obtained for precipitation as for temperature, but the connection is less clear (spatially noisier); also strong precipitation anomalies can be observed in regions remote from the Atlantic–European sector (not shown).

4 | CLIMATOLOGY OF QUASI-STATIONARY WAVES

In this section we highlight the variability of QSW activity, through the annual cycle, within each season, and from year to year, to better understand the climatological features of QSW variability.

The climatological distributions of mean QSW amplitudes in JJA and DJF show clear differences in the spatial pattern (Figure 2). One of these differences is a northward shift of QSW activity over Europe in JJA, which leads for example to the strong seasonal differences of QSW activity in the Mediterreanen region and the entry to the subtropical Asian jet. Unlike all other seasons, the main QSW activity in JJA is not concentrated in midlatitudes, but also occurs in high latitudes.

In addition to the different spatial patterns, one can also identify overall weaker mean QSW amplitudes during JJA. The distribution of QSW amplitudes in the Atlantic–European region (average 45°W to 45°E, 40 to 70°N; Figure 7a) shows that the weaker QSW mean amplitudes during JJA are not only a feature of the climatological mean fields (Figure 7b), but a general feature of QSWs in JJA. This difference is important if one intends to compare QSWs in different seasons. The extremely strong QSW for 9 August 2003 (solid annotated vertical line in Figure 7a) during the European heat wave in 2003 would not be identified as an extremely strong QSW if it had occurred in a different season (comparison with vertical dashed lines in Figure 7a). QSW amplitudes of different seasons cannot be compared directly. This seasonal difference in individual QSW strength is even more striking, as the amplitudes shown in Figure 7a are already the deviations from the seasonal varying climatological "background" QSW amplitude, which also reaches its minimum during summer (Figure 7b).

To investigate the variability of QSWs, we calculated the standard deviation of the daily envelope field for JJA and DJF (Figure 8). In general, the patterns resemble the mean climatological amplitudes, meaning that stronger variability tends to occur in regions of stronger mean amplitudes. However, there are some differences between the distribution of the mean climatological QSW amplitudes (contours) and the mean standard deviations (shading), most apparent in the region around Iceland and the Bering Strait during DJF.

To understand these differences we investigate the QSW pattern for the strongest (Figure 9a and b) and longest-lived QSWs (Figure 9c and d), because of the great influence of these particular QSWs on the overall pattern of QSW variability.

The patterns for these extreme QSWs in JJA (Figure 9a and c) look similar to the climatological pattern, which was expected from the similarity between the patterns of climatological mean amplitude and its standard deviation. However, during DJF there are prominent differences between the patterns of climatological mean and most extreme QSWs

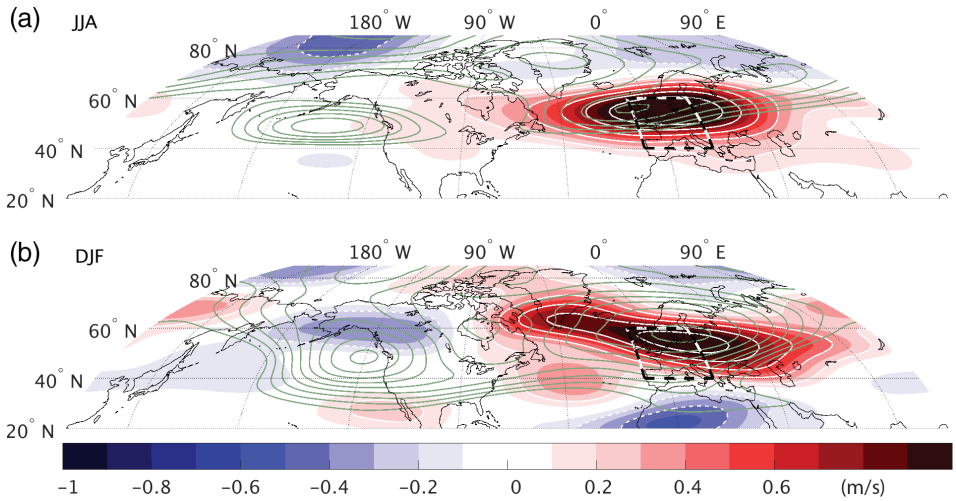

FIGURE 5 General connection between QSW amplitudes and temperature anomalies during (a) JJA and (b) DJF, showing the average anomalous (as deviations from daily climatology) QSW amplitudes in white contours (dotted for negative values, solid for positive values) and shading for the 50% strongest temperature anomalies (25% warmest and 25% coldest days). Temperature anomalies are defined by a 7-day running mean and a regional average over central Europe (dashed black-white box). Contours show the QSW amplitude climatology [Colour figure can be viewed at wileyonlinelibrary.com]

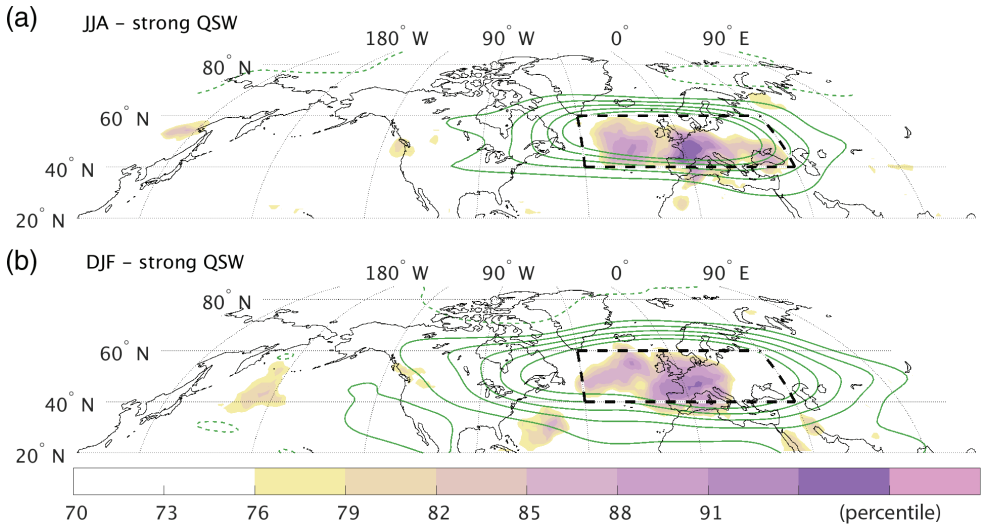

FIGURE 6 Temperature anomalies associated with the 30 strongest QSWs during (a) JJA and (b) DJF. Shading shows the composite of the modulus of temperature anomalies, measured in percentiles of a Monte Carlo simulation with the same number of dates of the same season. Extreme QSWs are identified by the highest average values over the midlatitude Atlantic–European region (dashed black-whiite box). Contours show the composite of anomalous QSW amplitudes (positive anomalies solid lines, negative anomalies dashed lines, with interval 1.2 m s^{-1}, and omitting the zero contour) [Colour figure can be viewed at wileyonlinelibrary.com]

(compare Figures 8b and 9b and d). The strongest and longest-lived QSWs do not occur in the regions of increased climatological mean amplitudes, but around the Bering Strait, at high latitudes over North America and in the Atlantic region from Europe towards Iceland and Greenland. These regions coincide with the regions of increased standard deviations away from the regions of high climatological mean amplitudes (Figure 8b). This suggests that the extreme QSWs are not only an amplified version of the climatological signal, but are represented by a different pattern with a different QSW evolution.

The dates of the strongest QSWs (as in Figure 9a and b) are associated with negative values of the AO index (in average below −1) and positive geopotential height anomalies at high latitudes. This is consistent with QSWs being associated with a reduced zonal-mean meridional gradient in geopotential height. This is of importance as this wave pattern is associated with strong temperature anomalies at high latitudes with overall cold anomalies over Eurasia.

5 | MIDLATITUDE MODES OF QSW VARIABILITY

This section is split into three parts. Section 5.1 shows the leading empirical orthogonal functions (EOFs) of the QSW dataset for the Northern Hemisphere and a discussion about their connection to European temperature anomalies.

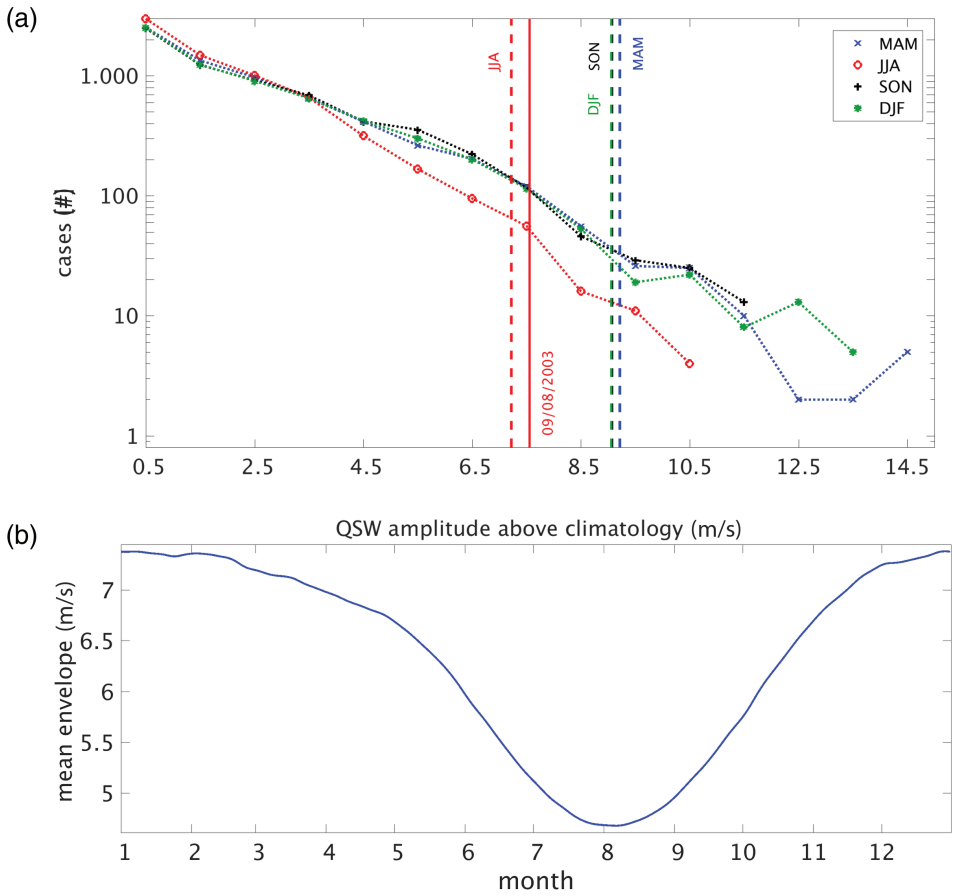

FIGURE 7 (a) Seasonal differences of QSW amplitudes above the daily based climatology in the European region (averaged over all gridpoints between 45°W to 45°E, 40 to 70°N). (b) The seasonal cycle of the mean envelope field in the Northern Hemisphere (averaged over all longitudes between 1°N and 85°N). In (a), the histogram bins are given by $(x, x + 1\ \mathrm{m\,s^{-1}}]$, with $x = 0.5, 1.5, 2.5, ..., 14.5\ \mathrm{m\,s^{-1}}$, and vertical dashed lines indicate the 99 percentile of QSW amplitudes for each season. [Colour figure can be viewed at wileyonlinelibrary.com]

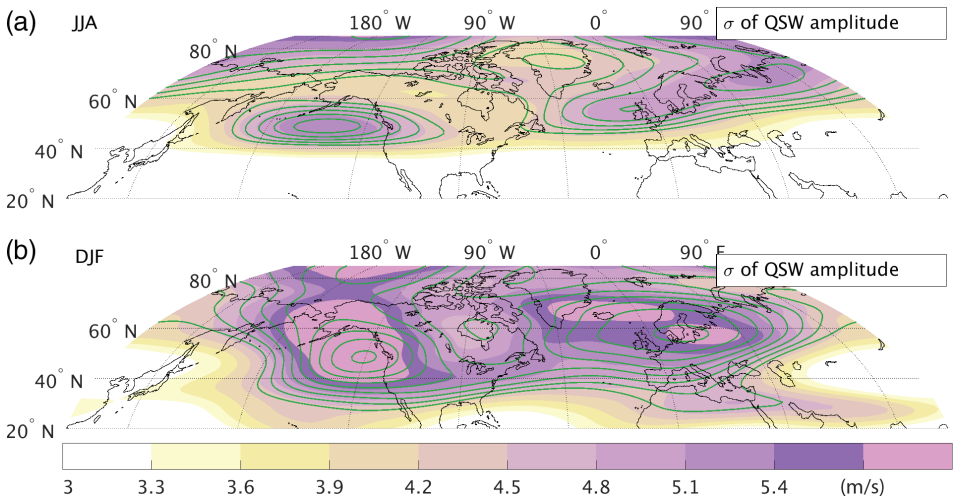

FIGURE 8 Spatial distribution of QSW activity during (a) summer (JJA) and (b) winter (DJF). Shading shows the standard deviation of the envelope field (12-hourly data), and contours show the climatological QSW amplitude, spaced every $0.5\ \mathrm{m\,s^{-1}}$, starting at $9\ \mathrm{m\,s^{-1}}$ [Colour figure can be viewed at wileyonlinelibrary.com]

The EOFs are the linear regression of the timeseries of the principal components onto the original data of the QSW amplitudes, leading the EOFs having the same units as the QSW amplitudes. Section 5.2 gives an overview of the connection of these EOFs and some important global pattern indices. Section 5.3 presents the results of a covariance analysis between European–Atlantic QSW activity and European temperatures, which show the most relevant QSW patterns in terms of European temperature anomalies.

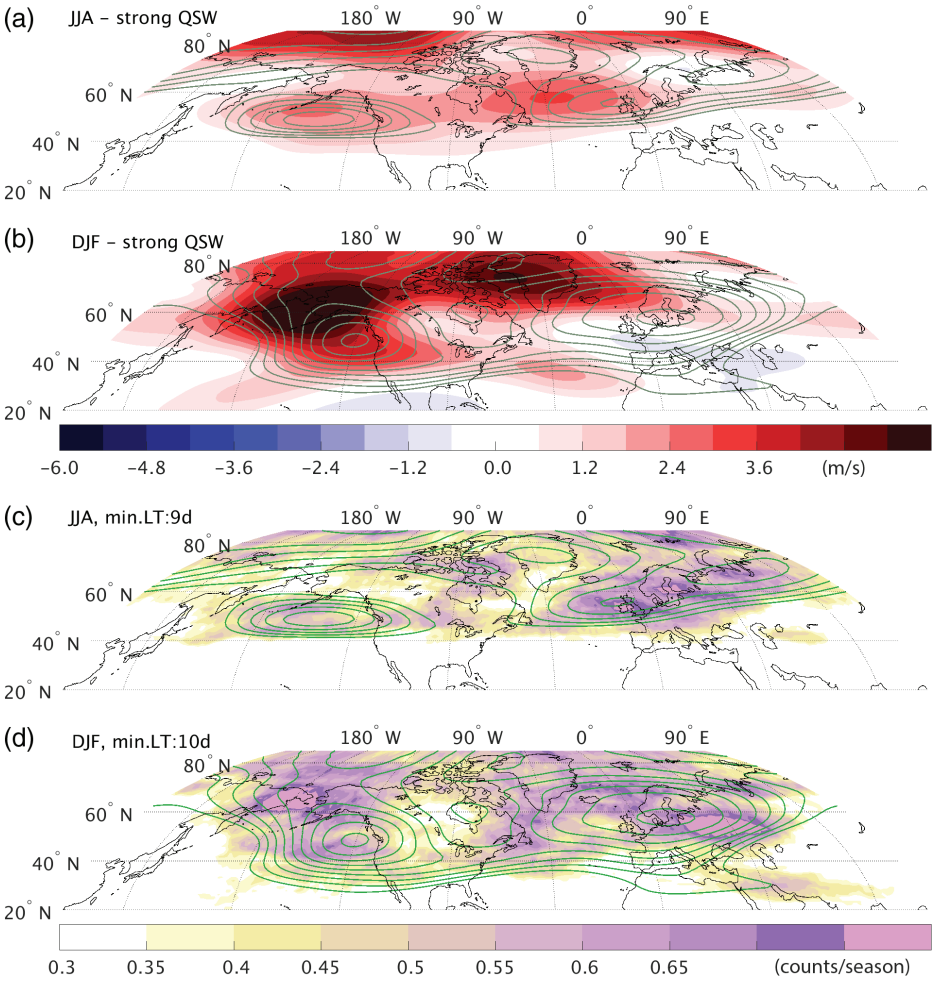

FIGURE 9 Regional and seasonal distribution of strongest and longest-lived QSWs. (a, b) show the anomalous QSW amplitude (shading) for the dates with the 5% strongest QSWs in (a) JJA and (b) DJF. (c, d) show the distribution of the number (shading) of QSW events with lifetimes of ≥ 10 days for (c) JJA and (d) DJF. The QSW lifetimes at each gridpoint are defined by the number of persistent days in which the QSW amplitude exceeds a value of 4 m s^{-1} above the daily climatology. Contours show the climatology of the QSW amplitudes for the relevant season, spaced every 0.5 m s^{-1}, starting with 9 m s^{-1} [Colour figure can be viewed at wileyonlinelibrary.com]

5.1 | EOF analysis of Northern Hemisphere QSW amplitudes

To investigate and understand the main modes of QSW amplitude variance, we calculate the first four leading EOFs of the QSW dataset between 20 and 85°N (four EOFs are retained following the "rule of thumb" given by North *et al.*, 1982). The results for JJA are shown in Figure 10 and for DJF in Figure 11.

The first EOF for JJA (Figure 10a, referred to here as *polar intensification*) shows that the main mode of variance is given by fluctuations in the strength of QSW activity at high latitudes. High QSW amplitudes at high latitudes is a specific feature of JJA; for the other seasons, the highest values of QSW amplitudes and variance of the amplitude are in midlatitudes. The second EOF (Figure 10b; *midlatitude intensification*) shows high/low QSW amplitudes in midlatitudes from the Pacific towards Asia, whereas EOF 3 (Figure 10c; *east–west high-latitude dipole*) and EOF 4 (Figure 10d; *east–west dipole*) represent two longitudinal dipole modes of QSW variance.

The extended zonal range of the JJA midlatitude intensification mode (Figure 10b) is similar to that observed for the composite QSW pattern associated with extreme high summer temperatures in Europe (Figure 3b), which suggests that this mode is associated with stronger warm anomalies in Europe. To confirm this, and to investigate the connection between the EOF modes and European temperatures in more detail, we correlated the principal component (PC) timeseries with the temperature signal, defined by a 7-day running mean, averaged over Europe (10°W to 20°E and 40 to 60°N). We do this correlation for different parts of the timeseries, using only the days with all warm anomalies ($T' > 0$), moderate warm anomalies ($T' > \sigma$ with σ being the standard deviation of the full temperature timeseries), all cold anomalies ($T' < 0$), moderate cold anomalies ($T' < -\sigma$), the modulus of all anomalies ($|T'|$) and the modulus of all moderate anomalies ($|T'| > \sigma$). This procedure should give us some insight into the association between temperature anomalies and the EOF patterns. The main features are discussed below (all of which are significant at the 95% confidence level) and

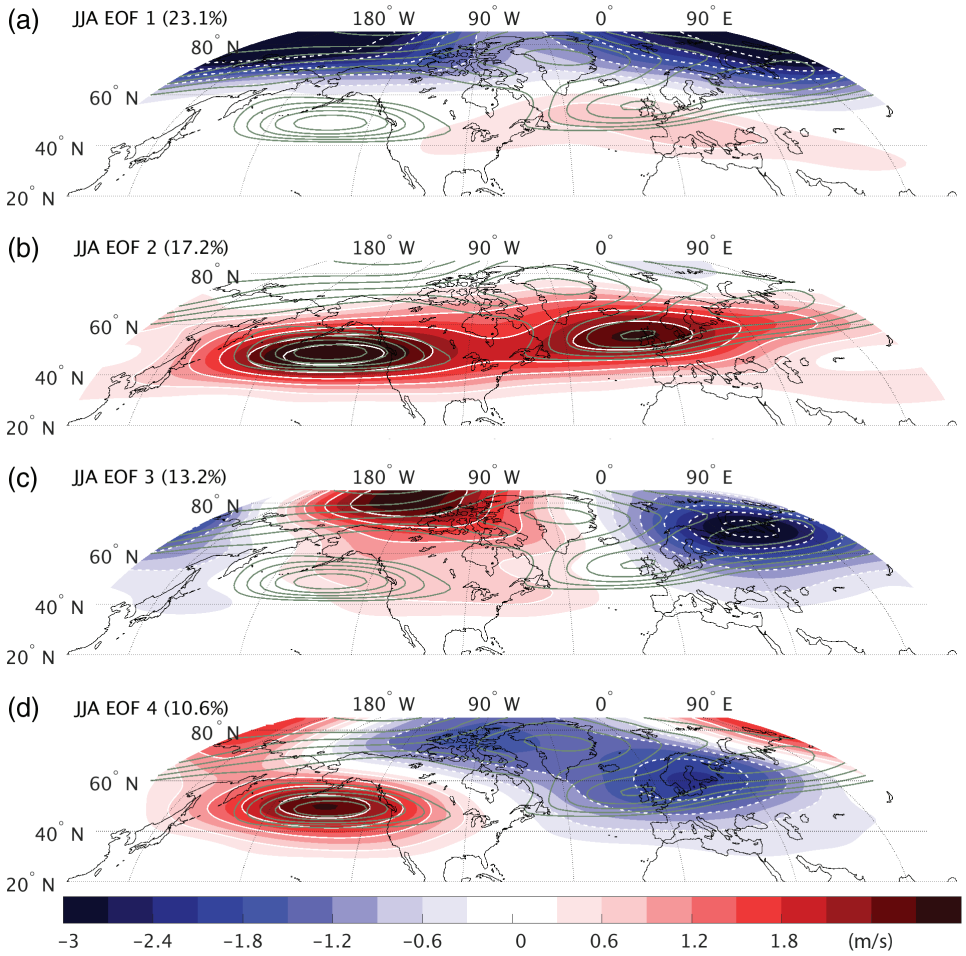

FIGURE 10 Leading EOF modes (a) 1, (b) 2, (c) 3 and (d) 4 of the daily anomalous QSW amplitudes shading with white contours, solid for positive values and dotted for negative values during JJA between 20 and 85°N for all longitudes. The percentage of the variance explained is given in the box in the upper left of each panel. Contours show the climatology of the QSW strength, spaced every 0.5 m s^{-1}, starting with 9 m s^{-1} [Colour figure can be viewed at wileyonlinelibrary.com]

a full table of correlation scores is provided in the Supporting information (Table S1).

High correlations can be found between warm anomalies and PC 4 (east–west dipole) and between both warm and cold anomalies and PC 2 (midlatitude intensification). The highest correlation of 0.31 is found for moderate warm anomalies and PC 2. This highlights the importance of zonally extended QSWs in the midlatitudes for European warm events. In particular, the 2003 heat wave is associated with anomalies of about 4 standard deviations for both the temperature anomaly and PC 2. PC 1 (polar intensification) shows weaker correlations with the temperature timeseries, but by calculating a timelag composite, one can see positive (negative) correlations prior to warm (cold) anomalies (not shown).

The DJF EOF modes are shown in Figure 11. The first EOF (Figure 11a; intensification) is associated with fluctuations in the overall strength of the QSW activity across the Northern Hemisphere with the maximum variance in the Pacific region and North America. The second EOF (Figure 11b; *north–south shift*) is represented by a meridional shift of QSW activity. The third EOF (Figure 11c; *east–west dipole*) shows a strong east–west dipole structure of the anomlous QSW amplitude and the fourth resembles a quadrupole structure (Figure 11d; *northwest–southeast quadrupole*), with a path of stronger QSW activity from the Pacific towards the northern part of the North Atlantic with weak QSW activity on its flanks.

Correlations between European temperature anomalies and the DJF EOF modes (as previously done for JJA) reveal a connection mainly with PC 2 (north–south shift) and PC 3 (east–west dipole). PC 1 (intensification) shows weaker correlations, but a timelag composite of the PC values shows positive values (increased QSW activity) during low temperatures and negative values (decreased QSW activity) after the occurrence of high temperatures. PC 3 (east–west dipole) shows correlations of ≈ 0.30 with cold anomalies and moderate warm anomalies. PC 2 (north–south shift) shows negative correlations ($\approx$ 0.2) for both warm and cold anomalies, indicating a clear separation of warm and cold anomalies with the negative and positive phase of PC 2. A northward shift of QSW activity is therefore associated with cold anomalies in Europe, whereas a southward shift of QSW activity is associated with warm anomalies in Europe. PC 4

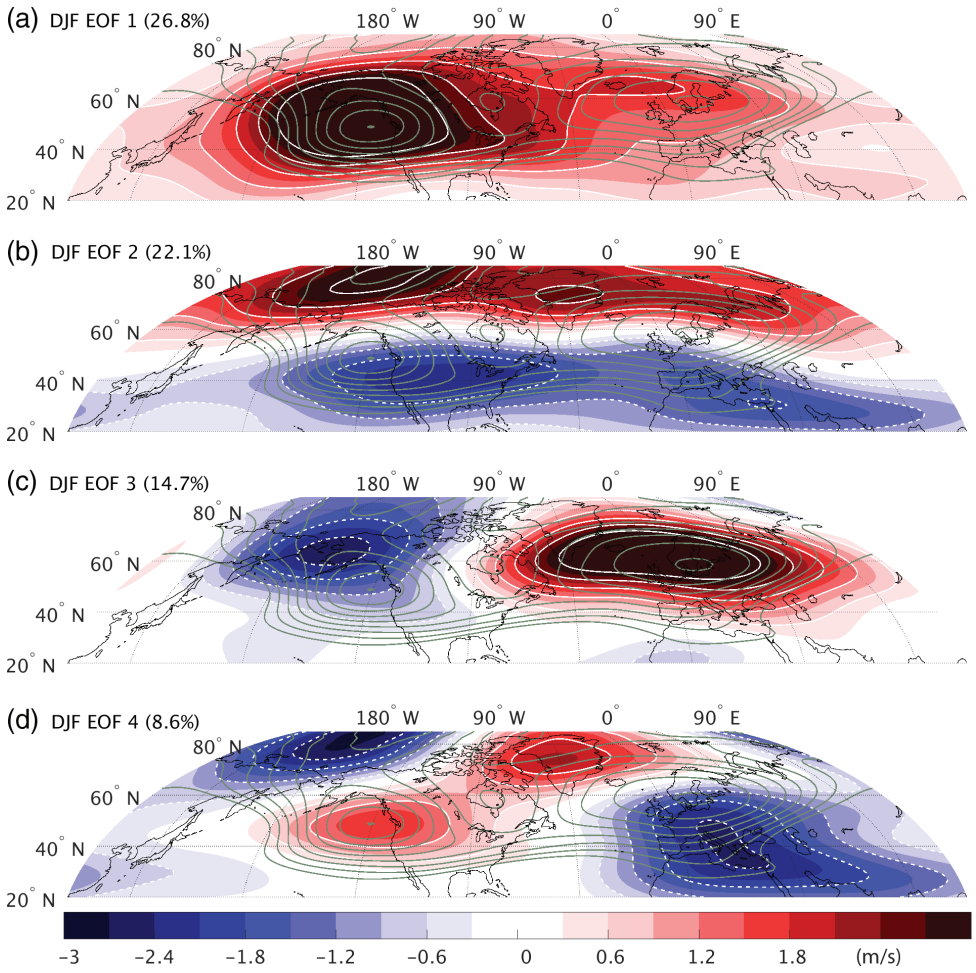

FIGURE 11 As Figure 10, but for DJF [Colour figure can be viewed at wileyonlinelibrary.com]

(northwest–southeast quadrupole) has in general small correlations for warm and cold anomalies, except for moderate warm anomalies (−0.26). This suggests that the QSW pattern represented by this EOF mode is normally not correlated with the temperature over Europe, but for strong warm anomalies a strong low-latitude QSW in the European/Mediterranean region may be often present, due to a meridional strongly amplified QSW.

Table 1 summarizes the main connections between the EOF modes in JJA and DJF with European temperatures. These EOFs are relevant, because they represent the main modes of QSW variance in the Northern Hemisphere and they show clear connections to European temperature anomalies.

5.2 | Connection between QSW EOFs and global pattern indices

Global pattern indices (GPI) are often used to characterize large-scale weather conditions. In this work we follow a different approach and use QSW patterns to characterize the large-scale conditions. This could be preferable because of the direct link to weather (section 3), which allows easier interpretation.

To investigate the connection between EOF QSW modes and GPIs, we calculated EOF composites for the positive and negative phase of the GPIs and correlated the monthly and seasonal averaged PC timeseries of the QSW EOFs with the associated GPIs. We used the NAO, the AO, the PNA and the ENSO in the Niño 3.4 region (Niño 3.4). The results are briefly summarized in the following. During summer there is no obvious direct connection between the QSW EOF modes and the chosen GPIs, therefore we will focus in the following on the connections for winter. A full table of results is provided in the Supporting information (Table S2), and the correlation scores discussed here are all significant at the 95% confidence level.

Niño 3.4 shows in both phases the strongest connection to EOF 3 (east–west dipole; correlation of −0.53 for seasonal averaged values) and the EOF 1 (intensification; −0.42 for seasonal correlation). This connection indicates increased QSW activity in the Pacific/North American region during its negative (La Niña) phase and vice versa. The PNA index shows a strong connection to EOF 1 (intensification) during its negative phase and has an overall strong correlation of −0.62 for the seasonal averaged values. This indicates that during the negative PNA one can observe increased midlatitude QSW activity. The NAO and

TABLE 1 Summary of the main connections between EOF modes of Northern Hemisphere QSW amplitudes and European temperature anomalies

Season	EOF mode	Connection to European temperature anomalies
JJA	Midlatitude intensification (EOF 2)	Increased QSW activity ↔ cold and (above all) warm anomalies
JJA	East–west dipole (EOF 4)	Increased Atlantic–European QSW activity ↔ warm anomalies
DJF	East–west dipole (EOF 3)	More Atlantic–European QSWs ↔ warm and cold anomalies
DJF	North–south shift (EOF 2)	QSWs shifted southward ↔ warm anomalies, QSWs shifted northward ↔ cold anomalies
DJF	Northwest–southeast quadrupole (EOF 4)	Strong warm anomalies associated with increased QSW acitivity around the Mediterranean

The summer and winter EOFs refer to the patterns in Figure 10 and 11 respectively.

AO show a strong connection to EOF 2 (north–south shift) with the strongest values during the negative phase, indicating increased high-latitude QSW activity for this phase. The correlations for the seasonal averaged values reach values of −0.52 (NAO) and −0.58 (AO). Further, the negative phase of the NAO and AO are also connected with EOF 4 (northwest–southeast quadrupole), which presumably comes from the north–south separation of QSW activity for this mode in the Atlantic/European region, similar to the north–south shift pattern (EOF 2).

5.3 | Covariance analysis between European temperatures and Atlantic/European QSW amplitudes

For further focus on the specific connections between QSW activity and European temperatures, we apply a maximum covariance (MC) analysis, following Czaja and Frankignoul (2002). The MC is calculated between daily Atlantic/European QSW amplitudes (100°W to 100°E and 20 to 85°N) and 7-day running means of temperature at 850 hPa in the European region (10°W to 20°E and 40 to 60°N). Maximizing the covariance between those two variables leads to an increase of the correlations between QSW MC modes and European temperatures and highlights the most relevant QSW patterns for European temperature anomalies (Figure 12).

As the sign of the covariance patterns is arbitrary and temperature anomalies are in general associated with increased QSW activity (section 3; Figure 5), we focus the discussion on the signal associated with increased QSW activity close to Europe.

The first mode in JJA (Figure 12a) resembles a mixture of EOFs 2 and 4 (midlatitude intensification and east–west dipole; Figure 10b and d) with the peak QSW activity over Europe. Warm anomalies over Europe are associated with this pattern of increased QSW activity (Figure 12a, right). However, this does not necessarily imply a particular phase structure or wavelength of the wave. Similar wave patterns can even have opposite phasing. This first mode is also similar to the composite QSW pattern of the 30 warmest events in Europe. A similarity is also found to the extreme cold-event composite for the second MC mode (Figure 12b), which indicates cold anomalies associated with increased QSW activity in the northern North Atlantic. This suggests that these wave patterns are not only relevant for extreme temperature events, but also for temperature anomalies in general, and that these extreme events are characterized by an amplified version of these patterns.

The first MC mode in DJF (Figure 12c) shows that cold anomalies are associated with high-latitude QSW activity in the extended Atlantic-European region. The second MC mode (Figure 12d) shows that temperature anomalies that lead to a decreased meridional temperature gradient are associated with increased QSW activity south of 65°N.

The first two modes together represent about 80% of the covariance, representing the main QSW patterns leading to increased persistent cold and warm anomalies in Europe. For winter, this percentage is even higher at more than 95%. The substantial variance explained by the first MC modes in each season suggests that the MC modes strongly influence seasonal temperature: a persistent QSW pattern in a particular year could lead to strong European temperature anomalies. To show this, we correlated the seasonal averaged PC timeseries of the QSW MC modes and the seasonal and spatial (10°W to 20°E, 40 to 60°N) averaged European temperatures (Figure 13). QSW amplitudes at one location often occur in pulses due to increasing and decreasing QSW amplitudes or just moving waves. Therefore we use only the 50% strongest values of the PC timeseries to calculate the seasonal average (i.e. we focus only on the contribution made by strong QSW periods). These seasonal averaged values show that the first MC mode defines a large contribution of the European temperature anomalies with correlations up to 0.52 in JJA (Figure 13a) and −0.63 in DJF (Figure 13b).

To get further insight into the connection between the first MC QSW mode and seasonal averaged temperature anomalies, we use for the seasonal average only the dates with positive or negative temperature anomalies. This results in higher correlations for the temperature anomalies associated with increased QSW activity for the leading MC mode in Fig 12a and c. In DJF this can be seen by a higher correlation for cold anomalies (−0.65) than for warm anomalies (−0.55), whereas in JJA only the correlation with warm anomalies (0.52) is statistically significant. To investigate the effects of long or frequent periods of decreased QSW activity on seasonal averaged temperatures, we now use the negative phase of the MC mode (lowest 50%). As expected, this leads to decreased correlations. In JJA no statistically significant seasonal correlations exist for the negative phase of the first MC

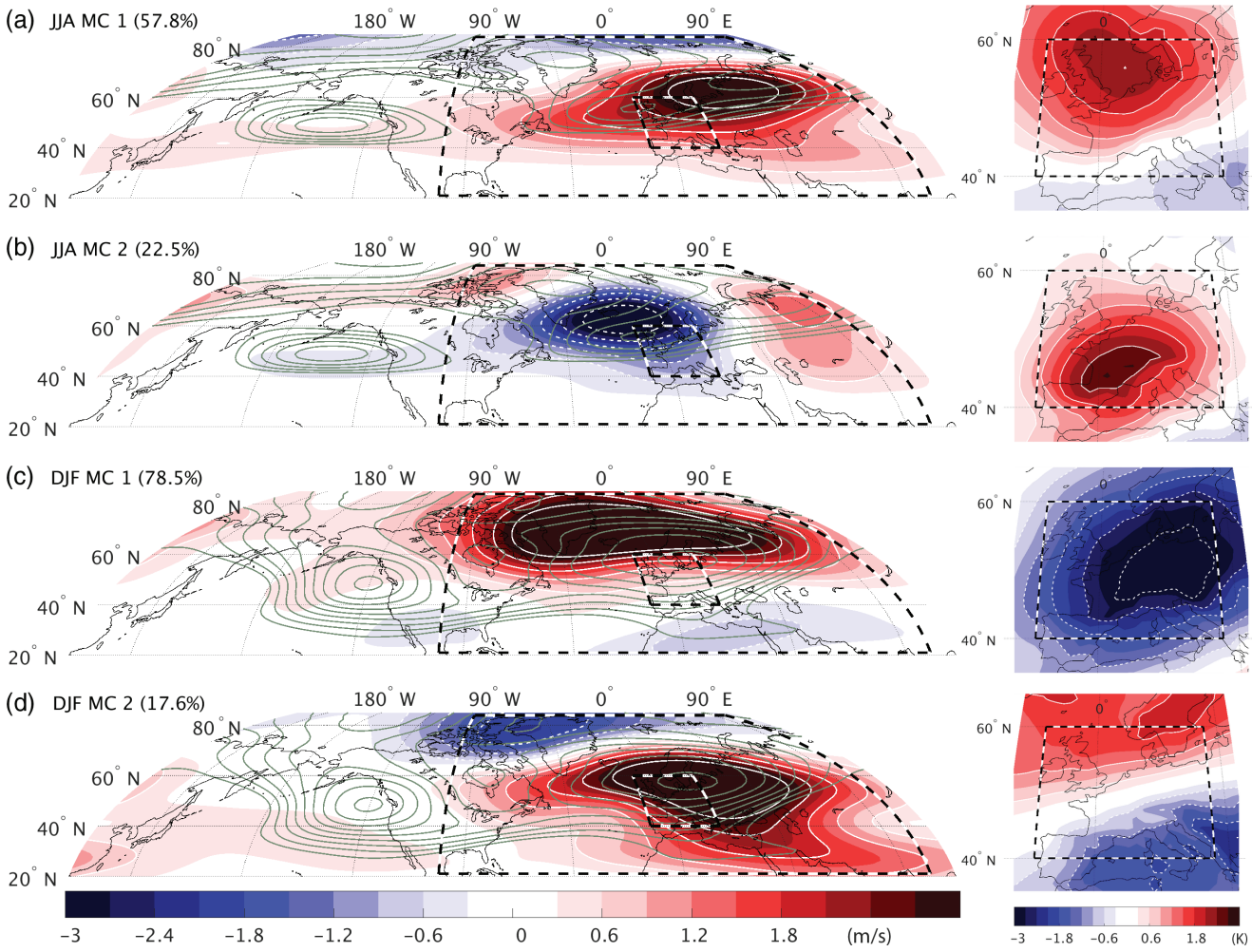

FIGURE 12 Leading MC modes (a) 1 and (b) 2 between the individual daily QSW amplitudes in the region 20 to 85°N and European temperatures at 850 hPa in the region 10°W to 20°E and 40 to 60°N during JJA. (c, d) are as (a, b), but for DJF. The anomalous QSW amplitudes are shown by white contours (dotted for negative values, solid for positive values) with shading. The percentage of the variance explained is given in the box in the upper left of each panel. Grey contours show the climatology of the QSW strength, spaced every 0.5 m s^{-1}, starting with 9 m s^{-1}. The right-hand panels show corresponding 7-day running means of temperature anomaly at 850 hPa [Colour figure can be viewed at wileyonlinelibrary.com]

mode, indicating that the first mode is mainly associated in its positive phase with warm anomalies, at least from a seasonally averaged perspective. For DJF the correlations are also weaker, but still reach values of 0.52 for warm anomalies and 0.56 for cold anomalies. This indicates that warm anomalies are associated with an absence of high-latitude QSW activity whereas for cold anomalies decreased high-latitude QSW activity is rather rare or weak. An absence of high-latitude QSW activity is therefore associated with an absence of low temperatures. The high correlations of all combinations of temperature anomalies with the DJF MC mode 1 demonstrate that this QSW pattern explains a substantial fraction of variance in European temperatures during DJF. The first MC mode somewhat resembles the north–south shift EOF (Figure 11) and consequently this EOF mode also shows an increased correlation of 0.50 with seasonal averaged European temperatures (not shown).

With the preceeding correlation analysis, we learnt something about the direct link (no timelag) and the seasonal averaged connection between the QSW patterns and temperature anomalies. To confirm some previous statement and to get further insight into the details of the connection between temperature anomalies and the MC modes, we now compute a ±30-day timelagged composite of the 15% warmest and 15% coldest days (Figure 14). The results are insensitive to the chosen percentage of days. This procedure should also reveal MC anomalies that are relevant for temperature anomalies, but which cannot be identified as such by using zero timelag.

This slightly different approach confirms the dominant influence of MC 1 with warm anomalies during JJA (Figure 14b) and cold anomalies during DJF (Figure 14c), with MC 1 slightly leading the temperature signal. In contrast, the cold anomalies in JJA (Figure 14a) and warm anomalies in DJF (Figure 14d) appear to be more associated with the MC 2 patterns, with the MC mode again leading the temperature signal slightly. Further, the MC 1 pattern in DJF indicates a persistent phase anomaly after the occurrence of the temperature anomalies (Figure 14c and d).

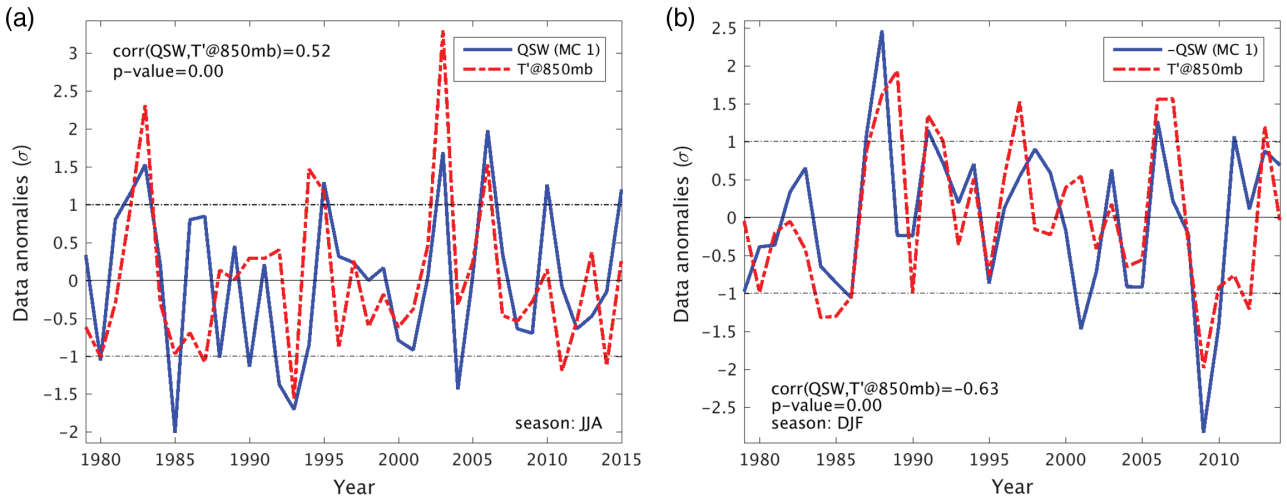

FIGURE 13 Connection between averaged temperature anomalies at 850 hPa (dashed) and the averaged first PC mode (solid, times^{-1} in panel b) in (a) JJA and (b) DJF. All variables are normalized by their respective standard deviations. Text in each panel gives the associated correlation and *p*-value of the timeseries [Colour figure can be viewed at wileyonlinelibrary.com]

6 | SUMMARY AND DISCUSSION

This paper makes use of a novel method to identify wave packets (Zimin *et al.*, 2003), which we refine to be applicable to investigate QSWs. We present results for the general behaviour of QSWs and their connection to European temperature anomalies and extreme weather events. We found a clear connection between extreme temperature events and QSWs. This suggests that extreme events are not only associated with localized blocking anticyclones, but zonally extended and persistent large-scale waves. We also found a connection between QSWs (or their absence) and extreme precipitation events, although the connection is not as clear as for temperature extremes. The connection between QSWs and weather extremes works in both directions: strong temperature anomalies are associated with strong QSWs and strong QSWs are associated with strong temperature anomalies. Furthermore, QSWs are not only relevant for extreme events, but they show a general connection to temperature anomalies, confirming the results of Screen and Simmonds (2014). Near-average weather is connected with weak or absent QSWs and strong anomalies are associated with increased QSW activity. This direct link between the large-scale pattern of QSWs and local weather highlights the importance of better understanding the general behaviour and evolution of specific classes of QSWs.

A specific characteristic of QSWs is the potential for a quasi-resonance mechanism (Petoukhov *et al.*, 2013). The QSW composite for the 30 warmest European temperature anomalies in JJA indicates that a QSW builds up more or less simultaneously at various regions, leading to a zonally elongated QSW. This finding gives some support for the quasi-resonance mechanism. However, for the other seasons and extreme cold events, quasi-resonance does not seem to be a dominant mechanism. Additional analysis (not shown) suggested that the QSWs associated with the European extreme warm anomalies may be connected with preceding flow anomalies in the Indian region and the Indian summer monsoon, consistent with the earlier studies of Ding and Wang (2005), though further investigation is required to explore this connection.

To increase our understanding of QSWs we investigated the climatological features and the main modes of variance of these waves. The climatology shows strong seasonal differences, with reduced QSW amplitudes during summer. The climatology peaks at the end of the storm tracks, similar to the Rossby wave-breaking climatology shown in Martius and Rivière (2016). This interesting similarity could give a hint of the importance of breaking propagating wave packets as QSW source or QSW amplification mechanisms. Sources of QSWs are not a topic in this paper, but will be investigated in future work. Differences in the QSW patterns in mean and variance reveal the importance of very strong and long-lived QSWs during winter over Iceland and the Bering Straits for the overall climatology, indicating that those anomalous QSWs evolve differently from the average QSW.

To investigate the variance of QSW patterns, an EOF analysis was applied and linked to European temperature anomalies. By doing so, specific QSW patterns could be identified that have a strong influence on European weather. Most prominent is the north-/southward shift of QSW activity in DJF: increased high-latitude QSW activity leads to lower temperatures and is essential for extreme low temperatures, while the absence of high-latitude activity or increased low-latitude QSW activity leads to higher temperatures. During summer, increased zonally extended QSW activity along the midlatitudes leads to stronger temperature anomalies, particularly warm anomalies.

To highlight the most relevant QSW patterns directly linked with strong temperature anomalies, a covariance analysis between European temperatures and Northern Hemisphere QSW amplitudes was applied. This analysis reveals the most

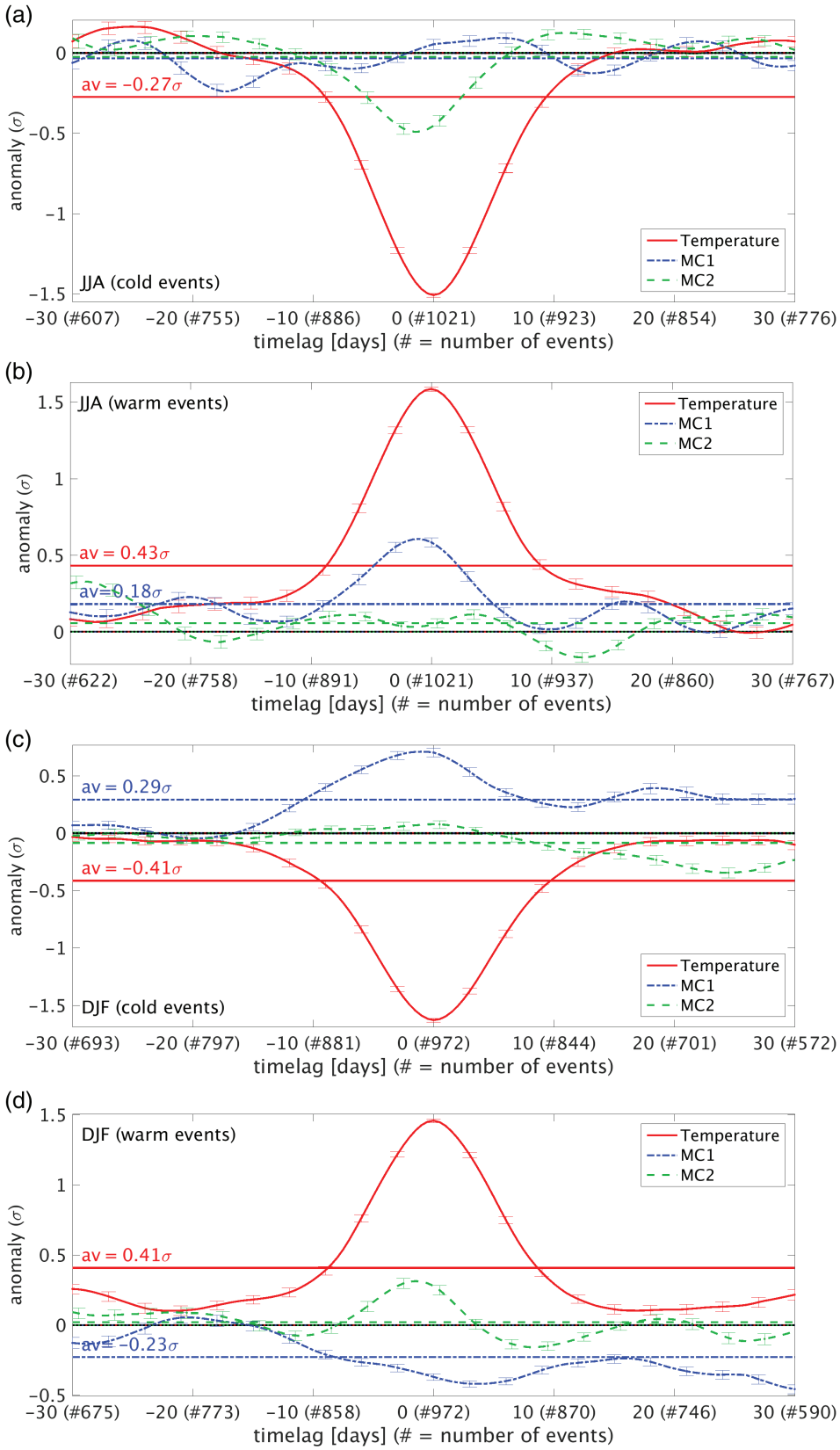

FIGURE 14 Timelag connection between leading MC modes 1 and 2 and European temperatures during (a, b) JJA and (c, d) DJF, showing timelag composites for the 15% (a, c) lowest and (b, d) highest temperature at 850 hPa, averaged over the region 10°W to 20°E and 40 to 60°N. Values are normalized by the standard deviation of the relevant season. Bars represent the standard error of the mean. Horizontal lines give the temporal averaged values for all timelags. Values larger than $\pm 0.1\sigma$ are given above these lines. Values in brackets show the number of events in the season; these decreases towards negative and positive timelags (dates outside of the season are not considered for the composite) [Colour figure can be viewed at wileyonlinelibrary.com]

important QSW patterns for European weather. Correlations between seasonal averaged QSW patterns and European temperatures showed that these QSW patterns are important not only for sub-seasonal periods of strong temperature anomalies, but also they strongly influence seasonal European weather conditions. This in particular highlights the importance of understanding the circumstances under which those patterns develop. This could be critical in a future climate with increased Arctic warming, as the large-scale baroclinicity can alter the occurrence and properties of QSWs (Cohen *et al.*, 2014), although the trends are complex and not well understood (Barnes, 2013). Such global features include, for example, sea-ice extent and tropical sea-surface temperatures (SSTs). Initial investigations suggest that some of the QSW patterns in summer (winter) are strongly correlated to spring (summer/autumn) sea-ice extent and one QSW pattern in DJF is very strongly correlated to tropical SST anomalies, starting as early as May (not shown). We intend to explore and confirm these potential connections in subsequent publications.

For a better comparability to other studies we applied our method to meridional wind at the 300 hPa pressure level. However, this does not fully take the seasonal differences in tropopause height into account. However, repeating our calculations using the meridional wind at 2 pvu as a better representation of the height of the dynamical tropopause leads qualitatively to the same results. The seasonal differences in the strength of the mean envelope field and QSW amplitudes are slightly reduced, but still clearly apparent.

In summary, our objective QSW identification method clearly shows that QSW patterns can be linked to overall large-scale weather conditions, to present a new viewpoint compared to traditional global pattern indices such as the NAO, AO, ENSO and the PNA. Indeed, there are strong connections between QSWs and such global patterns: the NAO and AO are strongly correlated with the north–south shift mode of QSW activity during DJF, leading in their negative phase to strong QSW activity at high latitudes, associated with rather low temperatures over Europe. The negative phase of ENSO and PNA in DJF lead to increased QSW activity in the Pacific and across the midlatitudes. However, unlike the global pattern indices, the QSW pattern directly links to synoptic weather conditions, allowing an easier interpretation of the underlying physics. Compared to maps of geopotential height or similar variables used to represent wave characteristics, our method does not suffer from issues of cancellation of non-stationary waves by temporal averaging. Even in the case of a potential driver triggering multiple QSWs which then slowly move downstream, averaging will not lead to decreased wave amplitudes and under-representation. This can be an important advantage when linking these QSWs to other phenomena or extreme events. It is therefore hoped that objective identification of QSW patterns could provide a useful new viewpoint for interpreting large-scale weather alongside more traditional measures such as regressed pattern indices or more commonly used variables.

ACKNOWLEDGEMENTS

We thank Sebastian Schemm and a second anonymous reviewer for their constructive comments, leading to improvements of the text. The data for the 12 hourly envelope fields between 1 June 1979 and 31 August 2015, without the smoothing in meridional direction (step (d) in Fig. 1), are available at the Centre for Environmental Data Analysis (Wolf *et al.* 2018). We acknowledge funding from the Natural Environment Research Council (NERC) for the ODYSEA project (grant number: NE/M006085/1). Nicholas P. Klingaman was funded by a NERC Independent Research Fellowship (NE/L010976/1).

ORCID

Gabriel Wolf https://orcid.org/0000-0001-5704-6550

REFERENCES

Barnes, E.A. (2013) Revisiting the evidence linking Arctic amplification to extreme weather in midlatitudes. *Geophysical Research Letters*, 40(17), 4734–4739. https://doi.org/10.1002/grl.50880.

Barnston, A. and Livezey, R. (1987) Classification, seasonality and persistence of low-frequency atmospheric circulation patterns. *Monthly Weather Review*, 115(6), 1083–1126. https://doi.org/10.1175/1520-0493(1987)115<1083:csapol>2.0.CO;2.

Black, E., Blackburn, M., Harrison, G., Hoskins, B.J. and Methven, J. (2004) Factors contributing to the summer 2003 European heatwave. *Weather*, 59(8), 217–223. https://doi.org/10.1256/wea.74.04.

Branstator, G. (2002) Circumglobal teleconnections, the jet stream waveguide, and the North Atlantic Oscillation. *Journal of Climate*, 15(14), 1893–1910. https://doi.org/10.1175/1520-0442(2002)015<1893:cttjsw>2.0.CO;2.

Carrera, M.L., Higgins, R.W. and Kousky, V.E. (2004) Downstream weather impacts associated with atmospheric blocking over the Northeast Pacific. *Journal of Climate*, 17(24), 4823–4830,4832–4839.

Catto, J.L., Shaffrey, L.C. and Hodges, K.I. (2010) Can climate models capture the structure of extratropical cyclones? *Journal of Climate*, 23(7), 1621–1635. https://doi.org/doi:10.1175/2009JCLI3318.1.

Cohen, J., Screen, J.A., Furtado, J.C., Barlow, M., Whittleston, D., Coumou, D., Francis, J., Dethloff, K., Entekhabi, D., Overland, J. and Jones, J. (2014) Recent Arctic amplification and extreme midlatitude weather. *Nature Geoscience*, 7(9), 627–637.

Czaja, A. and Frankignoul, C. (2002) Observed impact of Atlantic SST anomalies on the North Atlantic Oscillation. *Journal of Climate*, 15(6), 606–623. https://doi.org/10.1175/1520-0442(2002)015<0606:oioasa>2.0.CO;2.

Dee, D.P., Uppala, S.M., Simmons, A.J., Berrisford, P., Poli, P., Kobayashi, S., Andrae, U., Balmaseda, M.A., Balsamo, G., Bauer, P., Bechtold, P., Beljaars, A.C.M., van de Berg, L., Bidlot, J., Bormann, N., Delsol, C., Dragani, R., Fuentes, M., Geer, A.J., Haimberger, L., Healy, S.B., Hersbach, H., Hólm, E.V., Isaksen, L., Kållberg, P., Köhler, M., Matricardi, M., McNally, A.P., Monge-Sanz, B.M., Morcrette, J.-J., Park, B.K., Peubey, C., de Rosnay, P., Tavolato, C., Thépaut, J.-N. and Vitart, F. (2011) The ERA-Interim reanalysis: Configuration and performance of the data assimilation system. *Quarterly Journal of the Royal Meteorological Society*, 137(656, A), 553–597. https://doi.org/10.1002/qj.828.

Ding, Q. and Wang, B. (2005) Circumglobal teleconnection in the Northern Hemisphere summer. *Journal of Climate*, 18(17), 3483–3505. https://doi.org/10.1175/JCLI3473.1.

Enomoto, T., Hoskins, B.J. and Matsuda, Y. (2003) The formation mechanism of the Bonin high in August. *Quarterly Journal of the Royal Meteorological Society*, 129, 157–178. https://doi.org/10.1256/gj.01.211.

Glatt, I. and Wirth, V. (2014) Identifying Rossby wave trains and quantifying their properties. *Quarterly Journal of the Royal Meteorological Society*, 140, 384–396. https://doi.org/10.1002/qj.2139.

Glatt, I., Doernbrack, A., Jones, S.C., Keller, J., Martius, O., Mueller, A., Peters, D. and Wirth, V. (2011) Utility of Hovmöller diagrams to diagnose Rossby wave trains. *Tellus A*, 63(5), 991–1006. https://doi.org/10.1111/j.1600-0870.2011.00541.x.

Horel, J.D. (1985) Persistence of the 500 mb height field during Northern Hemisphere winter. *Monthly Weather Review*, 113(11), 2030–2042. https://doi.org/10.1175/1520-0493(1985)113<2030:potmhf>2.0.CO;2.

Hoskins, B.J. and Ambrizzi, T. (1993) Rossby wave propagation on a realistic longitudinally varying flow. *Journal of the Atmospheric Sciences*, 50(12), 1661–1671. https://doi.org/10.1175/1520-0469(1993)050<1661:rwpoar>2.0.CO;2.

Hovmöller, E. (1949) The trough-and-ridge diagram. *Tellus*, 1, 62–66. https://doi.org/10.1111/j.2153-3490.1949.tb01260.x.

Kornhuber, K., Petoukhov, V., Karoly, D., Petri, S., Rahmstorf, S. and Coumou, D. (2017) Summertime planetary wave resonance in the Northern and Southern Hemispheres. *Journal of Climate*, 30(16), 6133–6150. https://doi.org/10.1175/JCLI-D-16-0703.1.

Martius, O. and Rivière, G. (2016) Rossby wave breaking: Climatology, interaction with low-frequency climate variability, and links to extreme weather events. In: Li, J., Swinbank, R., Grotjahn, R. and Volkert, H. (Eds.) *Dynamics and Predictability of Large-Scale, High-Impact Weather and Climate Events*. Cambridge: Cambridge University Press. https://doi.org/10.1017/CBO9781107775541.006.

Masato, G., Woollings, T. and Hoskins, B.J. (2014) Structure and impact of atmospheric blocking over the Euro-Atlantic region in present-day and future simulations. *Geophysical Research Letters*, 41(3), 1051–1058. https://doi.org/10.1002/2013GL058570.

Nakamura, H., Nakamura, M. and Anderson, J. (1997) The role of high- and low-frequency dynamics in blocking formation. *Monthly Weather Review*, 125(9), 2074–2093. https://doi.org/10.1175/1520-0493(1997)125<2074:trohal>2.0.CO;2.

North, G., Bell, T., Cahalan, R. and Moeng, F. (1982) Sampling errors in the estimation of empirical orthogonal functions. *Monthly Weather Review*, 110(7), 699–706. https://doi.org/10.1175/1520-0493(1982)110<0699:seiteo>2.0.CO;2.

Pan, Z., Segal, M., Arritt, R., Chen, T. and Weng, S. (1999) A method for simulating effects of quasi-stationary wave anomalies on regional climate. *Journal of Climate*, 12(5), 1336–1343. https://doi.org/10.1175/1520-0442(1999)012<1336:amfseo>2.0.CO;2.

Petoukhov, V., Rahmstorf, S., Petri, S. and Schellnhuber, H.J. (2013) Quasi-resonant amplification of planetary waves and recent Northern Hemisphere weather extremes. *Proceedings of the National Academy of Sciences of the United States of America*, 110(14), 5336–5341. https://doi.org/10.1073/pnas.1222000110.

Plumb, R.A. (1985) On the three-dimensional propagation of stationary waves. *Journal of the Atmospheric Sciences*, 42, 217–229. https://doi.org/10.1175/1520-0469(1985)042<0217:ottdpo>2.0.CO;2.

Porter, D.F., Cassano, J.J. and Serreze, M.C. (2012) Local and large-scale atmospheric responses to reduced Arctic sea ice and ocean warming in the WRF model. *Journal of Geophysical Research*, 117. https://doi.org/10.1029/2011JD016969.

Sato, N. and Takahashi, M. (2006) Dynamical processes related to the appearance of quasi-stationary waves on the subtropical jet in the midsummer Northern Hemisphere. *Journal of Climate*, 19(8), 1531–1544. https://doi.org/10.1175/JCLI3697.1.

Screen, J.A. and Simmonds, I. (2014) Amplified mid-latitude planetary waves favour particular regional weather extremes. *Nature Climate Change*, 4(8), 704–709.

Takaya, K. and Nakamura, H. (2001) A formulation of a phase-independent wave-activity flux for stationary and migratory quasi-geostrophic eddies on a zonally varying basic flow. *Journal of the Atmospheric Sciences*, 58, 608–627. https://doi.org/10.1175/1520-0469(2001)058<0608:afoapi>2.0.CO;2.

Tang, Q., Zhang, X. and Francis, J.A. (2014) Extreme summer weather in northern midlatitudes linked to a vanishing cryosphere. *Nature Climate Change*, 4(1), 45–50. https://doi.org/10.1038/NCLIMATE2065.

Teng, H. and Branstator, G. (2017) Causes of extreme ridges that induce California droughts. *Journal of Climate*, 30(4), 1477–1492. https://doi.org/10.1175/JCLI-D-16-0524.1.

Trenberth, K. and Guillemot, C. (1996) Physical processes involved in the 1988 drought and 1993 floods in North America. *Journal of Climate*, 9(6), 1288–1298. https://doi.org/10.1175/1520-0442(1996)009<1288:ppiitd>2.0.CO;2.

Walsh, J.E. (2014) Intensified warming of the Arctic: Causes and impacts on middle latitudes. *Global and Planetary Change*, 117, 52–63. https://doi.org/10.1016/j.gloplacha.2014.03.003.

Whan, K., Zwiers, F. and Sillmann, J. (2016) The influence of atmospheric blocking on extreme winter minimum temperatures in North America. *Journal of Climate*, 29(12), 4361–4381. https://doi.org/10.1175/JCLI-D-15-0493.1.

Wolf, G. and Wirth, V. (2017) Diagnosing the horizontal propagation of Rossby wave packets along the midlatitude waveguide. *Monthly Weather Review*, 145(8), 3247–3264. https://doi.org/10.1175/MWR-D-16-0355.1.

Wolf, G., Brayshaw, D.J., Klingaman, N.P. and Czaja, A. (2018) Envelope field of Northern hemispheric upper tropospheric (300 hPa) quasi-stationary waves (June 1979 to August 2015). *Centre for Environmental Data Analysis*. https://doi.org/10.5285/c0c7998800414e46b6823dc75751bb4c.

Xie, Z., Black, R.X. and Deng, Y. (2017) The structure and large-scale organization of extreme cold waves over the conterminous United States. *Climate Dynamics*, 49(11), 4075–4088. https://doi.org/10.1007/s00382-017-3564-6.

Zimin, A.V., Szunyogh, I., Patil, D., Hunt, B.R. and Ott, E. (2003) Extracting envelopes of Rossby wave packets. *Monthly Weather Review*, 131(5), 1011–1017. https://doi.org/10.1175/1520-0493(2003)131<1011:eeorwp>2.0.CO;2.

Zimin, A.V., Szunyogh, I., Hunt, B.R. and Ott, E. (2006) Extracting envelopes of nonzonally propagating Rossby wave packets. *Monthly Weather Review*, 134(4), 1329–1333. https://doi.org/10.1175/MWR3122.1.

SUPPORTING INFORMATION

Additional supporting information may be found online in the Supporting Information section at the end of the article.

How to cite this article: Wolf G, Brayshaw DJ, Klingaman NP, Czaja A. Quasi-stationary waves and their impact on European weather and extreme events. *Q J R Meteorol Soc.* 2018;144:2431–2448. https://doi.org/10.1002/qj.3310

APPENDIX

CHOICE OF THE LATITUDE-DEPENDENT WAVENUMBER RANGE

In this Appendix we explain the choice of the latitude-dependent wavenumber range, which is used to calculate the QSWs. The latitude dependence is based on a cosine decay of the wavenumber range with increasing latitude.

The cosine decay is defined in such a way as to capture the main contribution of the power spectra of the wind field used to calculate the envelope field (as in Wolf and Wirth, 2017 for the envelope reconstruction of propagating wave packets). The underlying power spectra with the chosen wavenumber range can be seen in Figure A1. The black lines show the latitude-dependent wavenumber range used to reconstruct the envelope of the QSW. This wavenumber range includes

the wavenumbers derived from the barotropic Rossby wave dispersion relation

$$\omega = u\,k - \frac{\left(\beta - u_{yy}\right)\,k}{k^2 + l^2}, \tag{A1}$$

where u is the zonal background wind, k and l the zonal and meridional wavenumbers, the index $_y$ the meridional derivative and $\beta = f_y$ the meridional gradient of the Coriolis parameter. We can solve Equation (A1) by k^{i}, with $k^{\mathrm{i}} = k\,a\,\cos(\varphi)$ (k^{i} is used for the x-axis in Figure A1) and a the Earth radius. By doing so we obtain

$$k^{\mathrm{i}}\left(u, c_{\mathrm{p}}, \varphi, l^{\mathrm{i}}\right) = a\,\cos(\varphi)\sqrt{\frac{2\,\Omega\,\cos(\varphi)/a - u_{yy}}{\left(u - c_{\mathrm{p}}\right)} - \left(\frac{l^{\mathrm{i}}}{a}\right)^2}, \tag{A2}$$

where $c_{\mathrm{p}} = \omega/k$ is the zonal phase velocity and Ω is the angular velocity of Earth's rotation. Three possible scenarios of the function of k^{i} are given in Figure A1 by the three white lines. We obtain these lines if we use for Equation A2 a small meridional wavenumber ($l^{\mathrm{i}} = 2$), the zonal mean of the climatological zonal wind for u and a zonal phase velocity as fraction of u ($c_{\mathrm{p}} = 0.1\,u$ for the solid line and $c_{\mathrm{p}} = 0\,u$ and $0.5\,u$ for the two dashed lines).

This wavenumber range, given by the white lines, should represent the lower part of the chosen full wavenumber range (black lines). The input values for Equation A2 are very rough estimates of what we expect. The white lines in Figure A1 should suggest that with the chosen wavenumber range we are capturing the kind of waves which are of interest. For example, we chose the zonal mean of the zonal wind as the background wind. But in the presence of a QSW, we expect lower values of the background wind, while everywhere else the values can be higher. Therefore if we were to divide u by 2 in Equation A2, we would obtain higher values of k^{i}, capturing also more the right part of the wavenumber range (given by the black lines in Figure A1). Lower phase speeds have a smaller impact and would shift the white lines slightly further to the left in Figure A1 (which is also the case for higher meridional wavenumbers), whereas lower zonal wind speeds would lead to a stronger shift of the lines to the right into the higher wavenumber range inside the black lines. All in all, the considerations of this appendix should be sufficient to at least suggest that the chosen wavenumber range is reasonable.

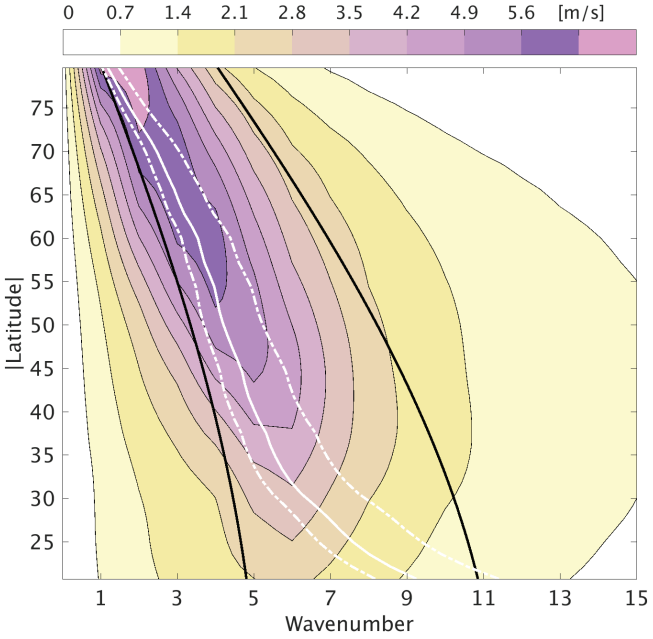

FIGURE A1 Latitude-dependent power spectra of the wind field used to calculate the QSW. Shading shows the power spectra of the deviation of the 15-day lowpass filtered meridional wind from its daily-based climatological value at 300 hPa for the years 1980 to 2015. Black lines represent the latitude-dependent wavenumber range used for the QSW calculation. White lines show the calculated wavenumbers by using the barotropic Rossby wave dispersion relation given in Equation A1 with a meridional wavenumber $l = 2$, the zonal averaged climatological zonal wind and three possible phase speeds. The white solid (dashed) line(s) result(s) from a phase speed equal to 0.1 (0 and 0.5) of the strength of the zonally averaged climatological zonal wind [Colour figure can be viewed at wileyonlinelibrary.com]